

Frustrated Dipole Order Induces Noncollinear Proper Ferrielectricity in Two Dimensions

Ling-Fang Lin,^{1,2} Yang Zhang,^{1,2} Adriana Moreo,^{2,3} Elbio Dagotto,^{2,3} and Shuai Dong^{1,*}

¹*School of Physics, Southeast University, Nanjing 211189, China*

²*Department of Physics and Astronomy, University of Tennessee, Knoxville, Tennessee 37996, USA*

³*Materials Science and Technology Division, Oak Ridge National Laboratory, Oak Ridge, Tennessee 37831, USA*

(Dated: January 17, 2022)

Within Landau theory, magnetism and polarity are homotopic, displaying a one-to-one correspondence between most physical characteristics. However, despite widely reported noncollinear magnetism, spontaneous noncollinear electric dipole order as ground state is rare. Here a dioxydihalides family is predicted to display noncollinear ferrielectricity, induced by competing ferroelectric and antiferroelectric soft modes. This intrinsic noncollinearity of dipoles generates unique physical properties, such as $\mathbb{Z}_2 \times \mathbb{Z}_2$ topological domains, atomic-scale dipole vortices, and negative piezoelectricity.

The Landau theory of phase transitions provides an elegant common framework for both magnetic and polar systems. The one-to-one correspondence between physical characteristics, such as ordered phases – ferromagnetic (FM) *vs* ferroelectric (FE) states, antiferromagnetic (AFM) *vs* antiferroelectric (AFE) states [see Figs. 1(a-b)], hysteresis loops, domains, and other properties is well recognized. However, ferrielectric (FiE) systems, with partially compensated collinear dipoles [Figs. 1(c-d)], are rare (except in liquid crystals and in a few solids like hybrid improper ferroelectrics [1] [2], while ferrimagnetic (FiM) materials are fairly common, e.g. Fe_3O_4 .

This incompleteness of dipole orders is even more dramatic with regards to *noncollinearity*. For magnets, spin noncollinearity has been widely studied [3, 4], leading to exotic magnetism-driven polarization (P) [5], skyrmions [6], and topological anomalous Hall effect [7]. There are several mechanisms to generate these crucial noncollinear spin orders. For example, in geometrically frustrated systems, such as two-dimensional (2D) triangular lattices, the AFM coupling between nearest-neighbor (NN) spins can generate the 120° order [3]. For other lattices, the exchange frustration, typically involving competition between NN FM (J_1) and next-nearest-neighbor (NNN) AFM (J_2) couplings, can generate magnetic cycloid or helical arrangements [4].

By contrast, the electric dipoles within a FE or AFE domain always tend to be parallel or antiparallel, aligned by the dipole-dipole interactions [8, 9]. Although slightly noncollinear dipole orders were proposed in a few FiEs, e.g. BaFe_2Se_3 and Pb_2MnWO_6 [10, 11], their noncollinearities are rigidly fixed by the local crystalline environment and, thus, can be trivially modulated. Noncollinear FiE phases were also predicted for strained BiFeO_3 [12–14], which has attracted much interest while waiting for experimental verification. In addition, dipoles can become noncollinear at some domain walls, as when forming flux-closure domains and even dipole vortices/skymions [15–19]. However, such non-

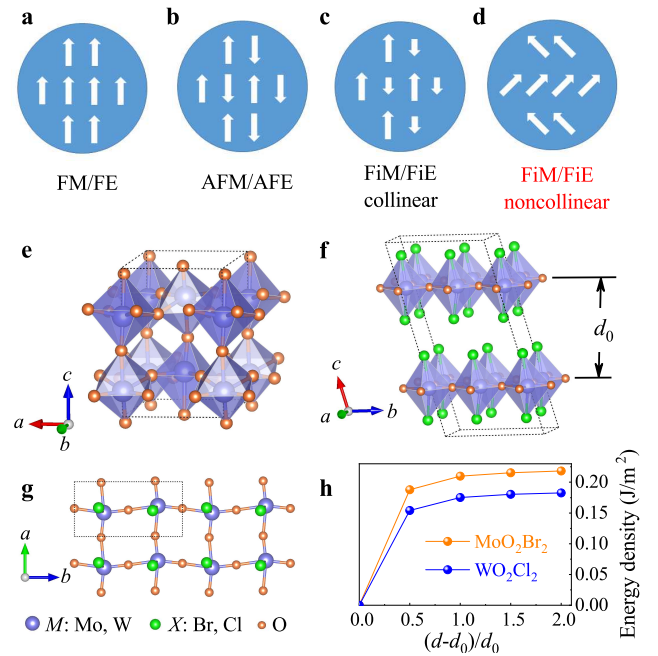


FIG. 1. (a-d) Sketch of the spin/dipole orders discussed in the text. (a) FM/FE parallel alignment; (b) AFM/AFE antiparallel alignment, fully compensated; (c-d) FiM/FiE: similar to (b) but with magnetization/polarization only partially compensated. (e, f) Structures of $\text{MO}_n\text{X}_{6-2n}$. (e) $n = 3$; (f) $n = 2$. The most stable vdW stacking is the A-B type. (g) Top view of a dioxydihalide monolayer (dash lines indicate a unit cell). (h) Cleavage energy density of the α phase.

collinearity is not a primary property of the FE state but driven by electrostatic effects from geometrically-confined boundary conditions.

Inspired by the “frustration” concept from magnets, here a series of 2D materials (MO_2X_2 , M : group-VI transition metal; X : halogen) is studied theoretically, which we predict can host intrinsic noncollinear electric dipole textures *spontaneously*.

2D FE monolayers (or few-layers) exfoliated from van

der Waals (vdW) layered materials are intrinsically superior at the nanoscale as compared with canonical three-dimensional (3D) FE materials [20–24]. In spite of this potential value, 2D FE materials remain rare [24] and their physical properties, such as domain structures, have not been well explored. This Letter demonstrates that these particular 2D noncollinear polar systems can provide an ideal platform to explore exotic polarity and topological domains beyond the standard collinear ferroelectricity, which may be crucial for domain wall nanoelectronics [25].

Physical properties.— Starting from the 3D MO_3 crystal [perovskite-like structure without A-site ions, see Fig. 1(e)], MO_2X_2 can be derived by replacing the apical O^{2-} oxygens by double halide ions X^- [Fig. 1(f)], forming a series of vdW layered materials. Further replacement of O^{2-} by X^- can lead to quasi-one-dimensional MOX_4 chains and to the zero-dimensional molecular limit MX_6 [see Figs. S1(a-b) in Supplementary Material (SM) [26]].

In this dioxidihalides family, WO_2Cl_2 and MoO_2Br_2 have been synthesized experimentally [27–29], while the crystal structures of the corresponding fluorides, iodides, and CrO_2X_2 are isomeric or unknown. Thus, in the following only WO_2Cl_2 and MoO_2Br_2 will be studied using density functional theory (DFT) [26]. Most previous studies of MO_2X_2 were devoted only to their chemical properties, while their physical properties were rarely addressed.

As shown in Fig. 1(g), each MO_2X_2 layer is composed of corner-sharing octahedra [29]. Contrary to most 2D materials which display compact honeycomb or triangular atomic arrangements, the “square” lattice of MO_2X_2 is spatially loose, which is advantageous for polar distortions. Due to the weak vdW interactions, there are two stacking modes for MO_2X_2 layers observed in experiments: the A-B stacking α -type (Fig. 1(f)) and the A-A stacking β -type [Fig. S1 in SM [26]], corresponding to the space groups Bb (No. 9) and $Pb2_1m$ (No. 26), respectively [27, 29]. The optimal distances (d_0 ’s) between adjacent layers are shorter in the α phases (see Table S1 in SM [26]), which are lower in energy than the β phases by 70 meV/W and 77 meV/Mo.

The cleavage energies were calculated to analyze whether it is possible to exfoliate MO_2X_2 monolayers, as shown in Fig. 1(h). For the α phase, the cleavage energies are 0.22 J/m² and 0.18 J/m² for MoO_2Br_2 and WO_2Cl_2 , respectively. For comparison, the cleavage energy for graphite is 0.325 J/m² theoretically [30] and 0.37 J/m² experimentally [31]. Thus, the exfoliation of a monolayer, or few-layers, from bulk MO_2X_2 should be feasible experimentally. Furthermore, our molecular dynamic simulation confirms the thermal stabilities of these monolayers at 300 K and 400 K (Fig. S2 in SM [26]).

Additional physical properties of MO_2X_2 monolayers and bulk forms are summarized in SM (Fig. S3 and Table.

S2) [26].

Noncollinear dipole order.— The paraelectric (PE) structure of MO_2X_2 is shown in Fig. 2(a), where all M ions are restored to the central positions of the O_4X_2 octahedra. In its phonon spectrum there are two imaginary-frequency branches, which will lead to spontaneous distortions. The symmetric B_{1g} (i.e. X_2^+) phonon mode at X (and Y) leads to AFE-type distortions [Fig. 2(b)]. The double-degenerate E_u (i.e. Γ_5^-) phonon mode at Γ leads to FE-type distortions [Fig. 2(c)]. Both these distortions lower the symmetry from tetragonal to orthorhombic.

The most striking physical result is that the cooperation of these two distortion modes, which resemble the exchange frustration in magnets, leads to a net FiE structure [Fig. 2(d)], which is dynamically stable according to its phonon spectrum. In this FiE state, the AFE and FE ordering directions are orthogonal, along the a and b axes, respectively. If the vdW d_0 is used as the thickness of a monolayer, the calculated net P ’s along the b axis are slightly larger than their bulk values (see Table S2 in SM [26]), themselves only a little larger than those of $BaTiO_3$ ($\sim 20 - 25 \mu C/cm^2$).

The d^0 rule (i.e. the formation of coordination bonds between M ’s empty d orbitals and O ’s $2p$ orbitals) should be the driving force for the polar distortions. This was confirmed by the Bader charge calculation [32]. As shown in Table S3 in SM [26], a small portion of valence electrons “leak” from O^{2-} to M^{6+} , accompanying the FiE distortions, which can also be visualized in Fig. 2(e). Although the d^0 rule is well known for FE/AFE perovskites, such as $BaTiO_3$ and $PbZrO_3$, interestingly none of the previously studied 2D FE systems belongs to this d^0 category [24], since none have perovskite-like structures.

The novel FiE state unveiled here is exotic. Due to the frustration between FE and AFE modes, here the local dipole moments are *noncollinear*, with a canting angle $\sim 129^\circ$ for WO_2Cl_2 ($\sim 128^\circ$ for MoO_2Br_2) between NN dipoles along the b axis. This unexpected noncollinearity leads to unique physics, as discussed below.

Domain & domain walls.— The DFT energy contour as a function of distortion modes for WO_2Cl_2 is shown in Fig. 3(a) and its Landau energy fitting can be found in SM [26]. For selected orthorhombic axes, four degenerate wells exist (characterized by the $\pm Q_1$ and $\pm Q_2$ of the X_2^+ and Γ_5^- modes), corresponding to the four domains: A^+ , A^- , B^+ , and B^- . An intuitive conclusion arising from Fig. 3(a) is that the favoured domain walls are between A^+/A^- , A^+/B^+ , B^+/B^- , and A^-/B^- , while domain walls between A^+/B^- or A^-/B^+ are highly energetic, thus unfavourable. A similar situation occurs in hexagonal manganites [33, 34], whose energy contour shows a Mexican-hat sixfold symmetry and, thus, prefers the well-known $\mathbb{Z}_2 \times \mathbb{Z}_3$ topological domain patterns [33, 34]. Contrary to WO_2Cl_2 , the collaborative modes in hexagonal manganites are the FE distortion and trimerization

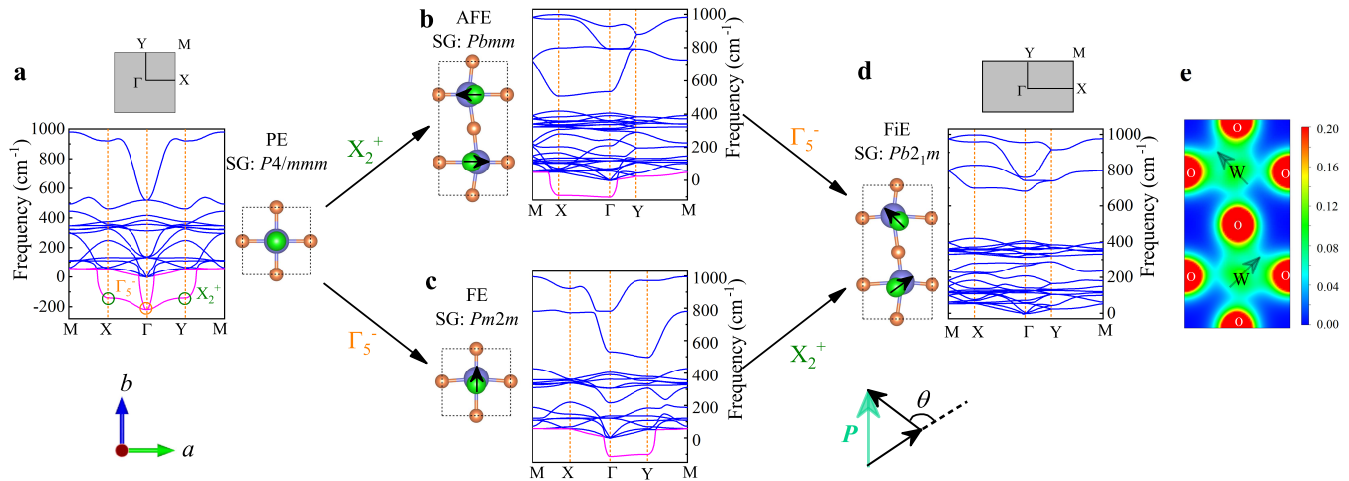


FIG. 2. Structural transitions of a MO_2X_2 monolayer. Shown are the phonon spectra of WO_2Cl_2 (those of MoO_2Br_2 are very similar, see Fig. S4 in SM [26]). The imaginary-frequency branches of phonons are displayed in pink. Grey square/rectangles are Brillouin zones. (a) The PE phase. The unstable distortion modes (X_2^+ & Γ_5^-) are indicated. (b) The intermediate AFE phase with the X_2^+ distortion mode. (c) The intermediate FE phase with the Γ_5^- distortion mode. (d) The resulting stable FiE ground state with both the X_2^+ & Γ_5^- distortion modes. The angles θ between NN dipoles (black arrows) along the b -axis are $\sim 129^\circ$. (e) Top view of the valence charge density of the WO_2 plane (integrated from -8 eV to the Fermi level). The d^0 orbitals of W^{6+} tend to form coordination bonds with two neighboring oxygens.

of the Mn-sublattice, not the AFE mode.

The possible FE and AFE domain walls in WO_2Cl_2 are shown in Fig. 3(b-c). Because the head-to-head and tail-to-tail charged domain walls are highly energetically unfavorable, we consider only the shoulder-by-shoulder charge-neutral domain walls. More details can be found in [26]. According to the DFT structural relaxations, these domain walls are atomically sharp, leading to distinct domains. The domain wall energies for FE and AFE domain walls are 1.6 meV/bond and 5.0 meV/bond for WO_2Cl_2 (11.5 meV/bond and 8.5 meV/bond for MoO_2Br_2), respectively.

As a consequence, it is natural to expect $\mathbb{Z}_2 \times \mathbb{Z}_2$ topological domain patterns in MO_2X_2 , as sketched in Fig. 3(d). If crystalline twinning and high-energetic charged domains can be excluded, the domain structure will be quite regular: the FE domain walls can only propagate along the b axis while the AFE domain walls can only propagate along the a axis, forming perpendicular cross points, namely atomic-scale \mathbb{Z}_4 antiphase vortices/antivortices. More details of domains and domain walls can be found in the SM [26].

In addition, atomic-scale dipole vortices/antivortices form at the FE domain walls, which is different to the dipole vortices in $PbTiO_3/SrTiO_3$ superlattices and $BiTiO_3$ nanostructures, whose size scale is much larger ($\sim 3 - 5$ nm) [16–19]. Our dipole vortices/antivortices are also different from those in the predicted $P2_12_12_1$ phase of strained $BiFeO_3$, whose atomic-scale dipole vortices/antivortices form a closely packed array with a fixed

position in the whole crystal [14], while ours exist only at some domain walls and thus are movable. The study of a dipole vortex, in correspondence to a magnetic vortex (or skyrmion) in magnetism, is an emerging topic in the field of polar materials. FiE MO_2X_2 can provide a superior playground for the dipole vortex due to its intrinsic non-collinearity.

Negative piezoelectricity.— For applications of FE materials, the switching of P 's are important physical properties. Interestingly, the switching paths for MO_2X_2 are nontrivial. As sketched in Fig. 4(a), the 180° reversal of the net P does not require the 180° flip of local dipoles, different from the plain FE cases. Instead, the collaborative $\sim 50^\circ$ rotations of local dipoles are enough, another unique property of the unveiled noncollinear ferrielectricity. As shown in Fig. 4(b), the AFE state can act as the nonpolar intermediate state, leading to a moderate energy barrier for P reversal. Comparing with their bulk values, the energy barriers do not change much, namely from 77 meV/f.u. (bulk) to 79 meV/f.u. (monolayer) for WO_2Cl_2 .

Another interesting issue is the 90° switching of P , which corresponds to the interchange of crystalline axes a and b . Two possible two-step paths are proposed to achieve this flop. As shown in Fig. 4(c), in each step half of the dipoles rotate while the other half remain fixed. Interestingly, the middle states just correspond to two kinds of domain walls, as sketched in Fig. 3(d). The corresponding switching energy barriers are plotted in Fig. 4(d), suggesting a slightly lower barrier for path I.

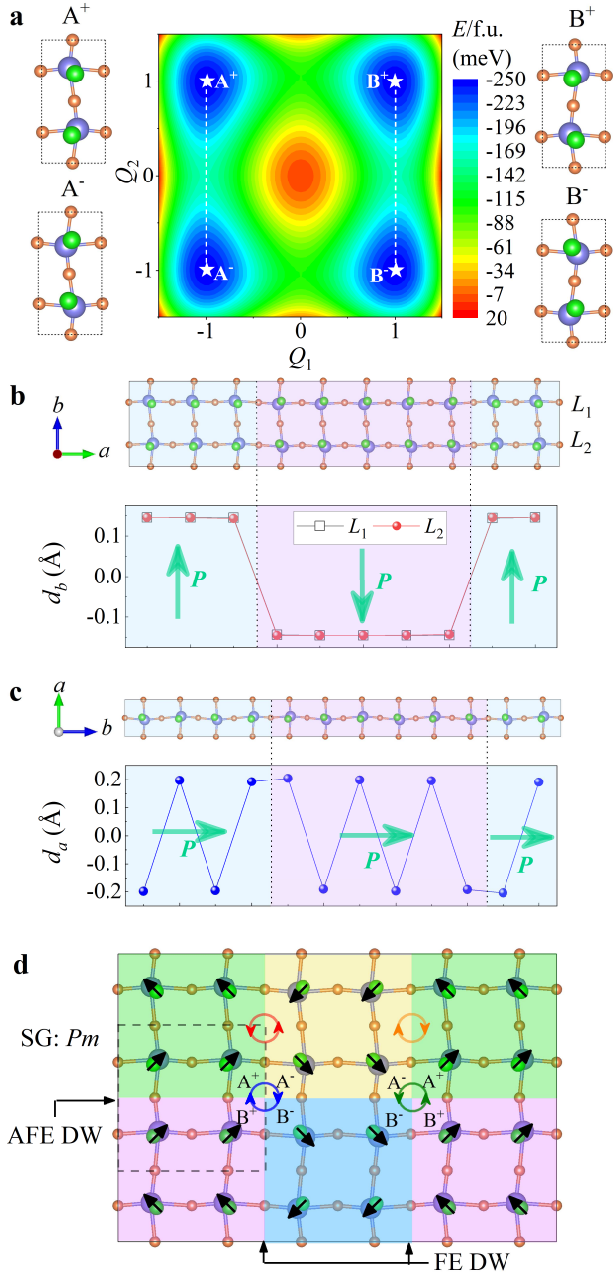


FIG. 3. Formation of $\mathbb{Z}_2 \times \mathbb{Z}_2$ domain textures in WO_2Cl_2 . Results in MoO_2Br_2 are qualitatively similar (Fig. S5 in SM [26]). (a) Contour plot of the energy varying Q_1 and Q_2 (amplitudes of X_2^+ and Γ_5^- modes). Q_1 and Q_2 are normalized to their optimized values. The indicated four degenerate lowest-energy wells correspond to the four domains (A^+ , A^- , B^+ , and B^-). $+/-$ indicate the sign of P along the $+b$ axis, while A/B distinguish the AFE configuration. (b-c) The atomically sharp domain walls: (b) FE domain walls; (c) AFE domain walls [d_a (d_b) are the displacements along the a -axis (b -axis)]. (d) Schematic of four-colored domains. The FE and AFE domain walls form perpendicular crossovers. Red (or orange) circles denote dipoles that form a vortex (antivortex) at the FE domain walls. The broken line square contain FE double-strips at AFE domain walls. The blue (green) circle is a topological $\mathbb{Z}_2 \times \mathbb{Z}_2$ antiphase domain emerging from one core. Two kinds of cores (vortex & antivortex) can be defined by the chirality of the domain phase.

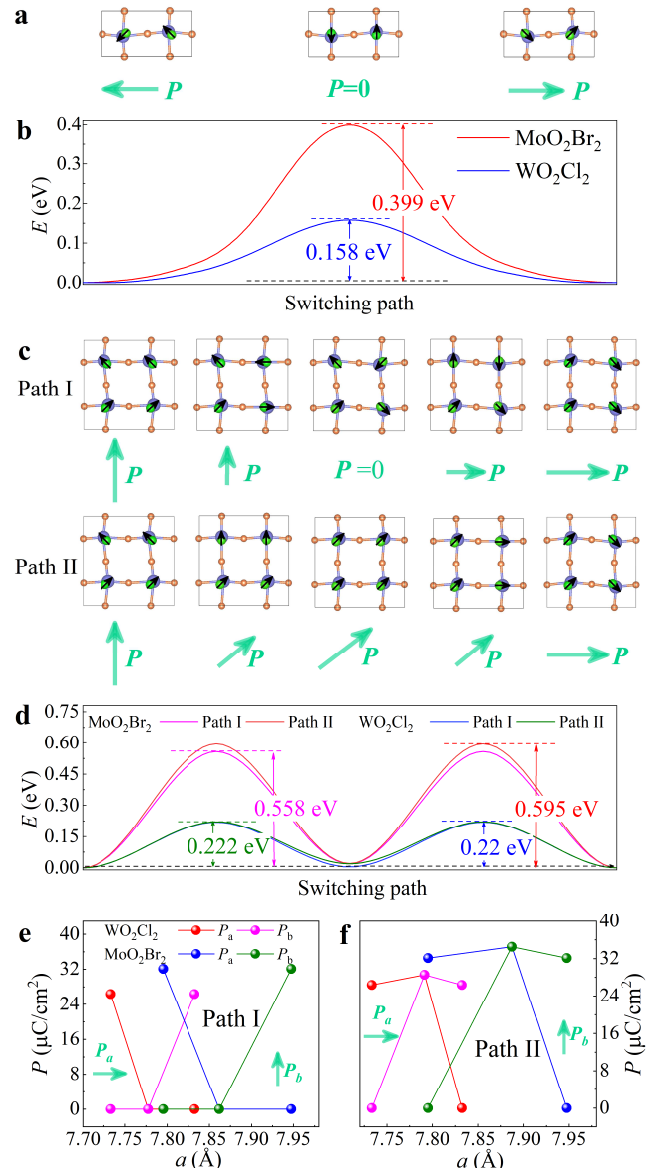


FIG. 4. Illustration of the unique FiE properties of MO_2X_2 . (a) 180° reversal path of the net P : FiE-AFE-FiE. (b) Energy barriers of the 180° reversal of P (for two M 's). (c) Two possible two-step paths for the 90° flop of P , namely the interchange of crystalline axes a and b . (d) Energy barriers for the 90° flop of P (for four M 's). (e-f) Correspondence between the a/b components of the P vector and the lattice constant a . The overall tendency is that P_a decreases with increasing a – negative piezoelectricity – although the actual process is unknown. (e) Path I. (f) Path II.

An interesting property of this 90° flop of P is the resulting negative piezoelectricity due to noncollinear ferroelectricity. Starting from the tetragonal PE state, the elongated axis of the orthorhombic FiE state is perpendicular to the direction of net P , i.e. $a > b$ for $P \parallel b$, which is unusual as compared with most ferroelectrics. This anomalous behavior is due to the noncollinearity

of local dipoles, since the a -axis component of each local dipole is larger than the b -axis component. Then, the 90° flop of P will lead to a negative piezoelectric coefficient d_{33} (see Figs. 4(e-f)), at least for the partial intermediate process during the 90° flop. In recent years, the existence of exotic negative piezoelectricity was predicted in special materials [35], but experimentally has only been observed in the organic FE polymer poly(vinylidene fluoride) (PVDF) [36] and CuInP_2S_6 [37].

Our calculations predict that the monolayer dioxydihalides MO_2X_2 's are promising 2D polar materials with exotic noncollinear ferrielectricity. The d^0 rule, which works in 3D ferroelectric perovskites but has not been found in 2D ferroelectrics before, is the driving force for the polar distortions. Noncollinear ferrielectric order persisting up to room temperature are expected. More importantly, the frustration between the FE and AFE modes generates an *intrinsically noncollinear dipole texture*, which leads to unique physics in the novel FiE state unveiled here, such as $\mathbb{Z}_2 \times \mathbb{Z}_2$ antiphase domain vortices, atomic-level dipole vortices at domain walls, negative piezoelectricity, and others. The key idea introduced here –the frustration of phonon instabilities– provide one more route to pursuit a variety of noncollinear dipole orders, such as cycloid dipole textures with particular chiralities or even dipole-based skyrmions. As a consequence of this noncollinearity, exotic physics is expected to emerge.

We thank Prof. Y. G. Yao and Dr. S. Guan for illuminating discussions. This work was primarily supported by the National Natural Science Foundation of China (Grant Nos. 11834002 and 11674055). A.M. and E.D. were supported by the U.S. Department of Energy (DOE), Office of Science, Basic Energy Sciences (BES), Materials Science and Engineering Division. L.F.L. and Y.Z. were also supported by the China Scholarship Council. We thank the Tianhe-II of the National Supercomputer Center in Guangzhou (NSCC-GZ) and the Big Data Center of Southeast University for providing the facility support on the numerical calculations.

* Corresponding author. Email: sdong@seu.edu.cn

- [1] N. A. Benedek and C. J. Fennie, Phys. Rev. Lett. **106**, 107204 (2011).
- [2] J. F. Scott, F. Morrison, A. M. Slawin, P. Lightfoot, R. Clulow, A. S. Gherson, A. M. Bumstead, J. Gardner, S. C. Capelli, M. R. Probert, et al., Physical Review B **95**, 094119 (2017).
- [3] A. P. Ramirez, Annu. Rev. Mater. Sci. **24**, 453 (1994).
- [4] S.-W. Cheong and M. Mostovoy, Nat. Mater. **6**, 13 (2007).
- [5] T. Kimura, Annu. Rev. Mater. Res. **37**, 387 (2007).
- [6] N. Nagaosa and Y. Tokura, Nat. Nanotechnol. **8**, 899 (2013).
- [7] N. Nagaosa, J. Sinova, S. Onoda, A. H. MacDonald, and N. P. Ong, Rev. Mod. Phys. **82**, 1539 (2010).
- [8] M. Dawber, K. M. Rabe, and J. F. Scott, Rev. Mod. Phys. **77**, 1083 (2005).
- [9] K. M. Rabe, C. H. Ahn, and J.-M. Triscone, eds., *Physics of Ferroelectrics: A Modern Perspective* (Berlin: Springer, 2007).
- [10] S. Dong, J.-M. Liu, and E. Dagotto, Phys. Rev. Lett. **113**, 187204 (2014).
- [11] F. Orlandi, L. Righi, R. Cabassi, D. Delmonte, C. Pernechele, and F. Bolzoni, Inorg. Chem. **53**, 10283 (2014).
- [12] Y. Yang, W. Ren, M. Stengel, X. Yan, and L. Bellaiche, Physical review letters **109**, 057602 (2012).
- [13] Y. Yang, J. Íñiguez, A.-J. Mao, and L. Bellaiche, Physical review letters **112**, 057202 (2014).
- [14] S. Prosandeev, I. A. Kornev, and L. Bellaiche, Physical review letters **107**, 117602 (2011).
- [15] C.-L. Jia, K. W. Urban, M. Alexe, D. Hesse, and I. Vrejoiu, Science **331**, 1420 (2011).
- [16] I. I. Naumov, L. Bellaiche, and H. Fu, Nature **432**, 737 (2004).
- [17] Y. Nahas, S. Prokhorenko, L. Louis, Z. Gui, I. Kornev, and L. Bellaiche, Nature communications **6**, 8542 (2015).
- [18] A. K. Yadav, C. T. Nelson, S. L. Hsu, Z. Hong, J. D. Clarkson, C. M. Schlepüetz, A. R. Damodaran, P. Shafer, E. Arenholz, L. R. Dedon, D. Chen, A. Vishwanath, A. M. Minor, L. Q. Chen, J. F. Scott, L. W. Martin, and R. Ramesh, Nature **530**, 198 (2016).
- [19] S. Das, Y. Tang, Z. Hong, M. Gonçalves, M. McCarter, C. Klewe, K. Nguyen, F. Gómez-Ortiz, P. Shafer, E. Arenholz, et al., Nature **568**, 368 (2019).
- [20] K. Chang, J. W. Liu, H. C. Lin, N. Wang, K. Zhao, A. M. Zhang, F. Jin, Y. Zhong, X. P. Hu, W. H. Duan, Q. M. Zhang, L. Fu, Q.-K. Xue, X. Chen, and S.-H. Ji, Science **353**, 274 (2016).
- [21] F. C. Liu, L. You, K. L. Seyler, X. B. Li, P. Yu, J. H. Lin, X. W. Wang, J. D. Zhou, H. Wang, H. Y. He, S. T. Pantelides, W. Zhou, P. Sharma, X. D. Xu, P. M. Ajayan, J. L. Wang, and Z. Liu, Nat. Commun. **7**, 12357 (2016).
- [22] W. J. Ding, J. B. Zhu, Z. Wang, Y. F. Gao, D. Xiao, Y. Gu, Z. Y. Zhang, and W. G. Zhu, Nat. Commun. **8**, 14956 (2017).
- [23] Y. Zhou, D. Wu, Y. Zhu, Y. Cho, Q. He, X. Yang, K. Herrera, Z. Chu, Y. Han, M. C. Downer, H. Peng, and K. Lai, Nano Lett. **17**, 5508 (2017).
- [24] M. Wu and P. Jena, Wiley Interdiscip. Rev.: Comput. Mol. Sci. **8**, e1365 (2018).
- [25] G. Catalan, J. Seidel, R. Ramesh, and J. F. Scott, Rev. Mod. Phys. **84**, 119 (2012).
- [26] See Supplemental Materials for more results and discussions.
- [27] O. Jarchow, F. Schröder, and H. Schulz, Z. Anorg. Allg. Chem. **363**, 58 (1968).
- [28] A. R. Armstrong, J. Canales, and P. G. Bruce, Angew. Chem. Int. Ed. **116**, 5007 (2004).
- [29] T. Schustereit, T. Schleid, and I. Hartenbach, Z. Anorg. Allg. Chem. **637**, 1159 (2011).
- [30] N. Mounet, M. Gibertini, P. Schwaller, D. Campi, A. Merkys, A. Marrazzo, T. Sohier, I. E. Castelli, A. Cepellotti, G. Pizzi, and N. Marzari, Nat. Nanotechnol. **13**, 246 (2018).
- [31] W. Wang, S. Dai, X. Li, J. Yang, D. J. Srolovitz, and Q. Zheng, Nat. Commun. **6**, 7853 (2015).

- [32] G. Henkelman, A. Arnaldsson, and H. Jónsson, *Comput. Mater. Sci.* **36**, 354 (2006).
- [33] T. Choi, Y. Horibe, H. T. Yi, Y. J. Choi, W. Wu, and S.-W. Cheong, *Nat. Mater.* **9**, 253 (2010).
- [34] S. Artyukhin, K. T. Delaney, N. A. Spaldin, and M. Mostovoy, *Nat. Mater.* **13**, 42 (2014).
- [35] S. Liu and R. E. Cohen, *Phys. Rev. Lett.* **119**, 207601 (2017).
- [36] I. Katsouras, K. Asadi, M. Li, T. B. vanDriel, K. S. Kjær, D. Zhao, T. Lenz, Y. Gu, P. W. M. Blom, D. Damjanovic, M. M. Nielsen, and D. M. de Leeuw, *Nat. Mater.* **15**, 78 (2015).
- [37] L. You, Y. Zhang, S. Zhou, A. Chaturvedi, S. A. Morris, F. Liu, L. Chang, D. Ichinose, H. Funakubo, W. Hu, *et al.*, *Science advances* **5**, eaav3780 (2019).